Supporting Information

Bioresource-Derived Colloidal Nitrogen-Doped Graphene Quantum Dots as Ultrasensitive and Stable Nanosensors for Cancer and Neurotransmitter Biomarkers

Yan-Yi Chen[1], Darwin Kurniawan[1], Seyyed Mojtaba Mousavi[1], Pavel V. Fedotov[2,3], Elena D. Obraztsova[2,3], and Wei-Hung Chiang[1]*

[1]Department of Chemical Engineering, National Taiwan University of Science and Technology, Taipei 10607 Taiwan

[2]A.M. Prokhorov General Physics Institute, Vavilov Str. 38, Moscow, 119991 Russia

[3]Moscow Institute of Physics & Technology, 9 Institutskiy per., Dolgoprudny, Moscow Region, 141701, Russia

*Corresponding author: E-mail address: whchiang@mail.ntust.edu.tw (W.H.C.).

S1. Purification and characterizations

Purification

After the synthesis, the colloidal NGQD was neutralized with 0.1 M NaOH. Then, acetone with around double volume of the NGQD solution was added to precipitate the unreacted chitosan. The suspension was centrifuged at 6000 rpm for 10 min to separate the unreacted chitosan precipitate and the mixture of NGQD solution and acetone. The NGQD solution was further filtered using vacuum filtration to ensure that there was no chitosan residue. The solution obtained was finally evaporated using a rotary evaporator. All solutions were evaporated and a small amount of ethanol was added to redisperse the NGQDs adhering to the vial walls, followed by another evaporation to obtain fine NGQD powder.

Characterizations

The absorption spectra were recorded with a matched pair of quartz cuvettes (1 cm path length) at room temperature. Background measurement was performed before every measurement. The Raman shifts were calibrated with a silicon wafer having a Raman peak at 520 cm^{-1}. The TEM specimen was prepared by drop-casting the NGQD solution onto a carbon-coated copper grid (400 mesh, Ted Pella) and dried at 50 °C for 3 days.

S2. Raman and FTIR measurements of NGQDs and chitosan

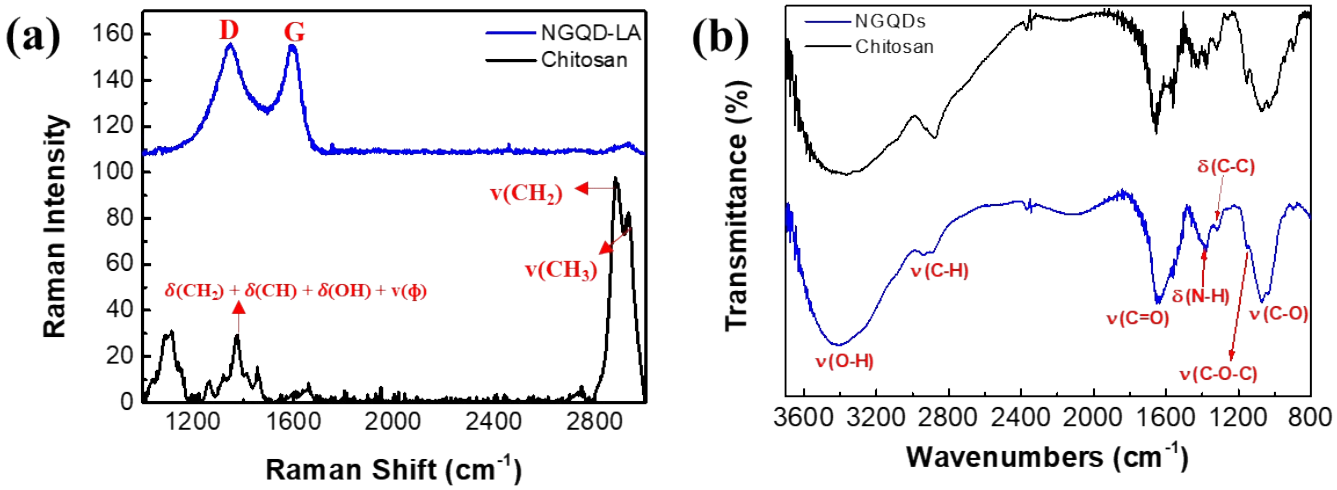

Figure S1. (a) Raman and (b) FTIR spectra of NGQDs and Chitosan.

Two characteristic peaks of CH_3 and CH_2 vibration and stretching were respectively observed at 2930 and 2880 cm^{-1} in chitosan (**Figure S1a**). The peak observed at 1373 cm^{-1} coincides with several other weaker peaks, which can be attributed to the vibration of CH_3, CH_2, and OH in the pyranose ring of chitosan.[1] Meanwhile, the generated NGQDs show two strong Raman bands, including the G-band at 1598 cm^{-1} and D-band at 1347 cm^{-1}, corresponding to a highly crystalline graphene structure with some disorders originating from nitrogen dopants, vacancies induced by non-graphitic nitrogen-doping, and edge effects in NGQDs.[2] Therefore, the average intensity ratio of D-band and G-band (I_D /I_G) was calculated to be 1.02 ± 0.06, suggesting disordered but highly crystalline carbon atoms, which further confirms that NGQDs contain a large number of defects in the form of edge, and surface functional groups. No observable characteristic Raman peaks of chitosan were observed, indicating NGQDs with high purity that can improve their practicality, especially for biosensing applications.[3]

FTIR measurements confirmed the presence of surface functional groups in the synthesized NGQDs, as shown in **Figure S1b**. The benzene ring of NGQDs has C-H stretching vibration peaks at 2947 cm^{-1}. The existence of N doping in the carbon lattice is from the pyridine (C=N) stretching vibrations and the C-NH bending vibrations at 1382 cm^{-1}. Furthermore, at 3400 cm^{-1} (-OH), 1639 cm^{-1} (C=O), 1320 cm^{-1} (C-C), 1080 cm^{-1} (CO) and 1157 cm^{-1} (COC) are confirmed by the vibrational stretching peaks.[4]

S3. XPS measurements of NGQDs

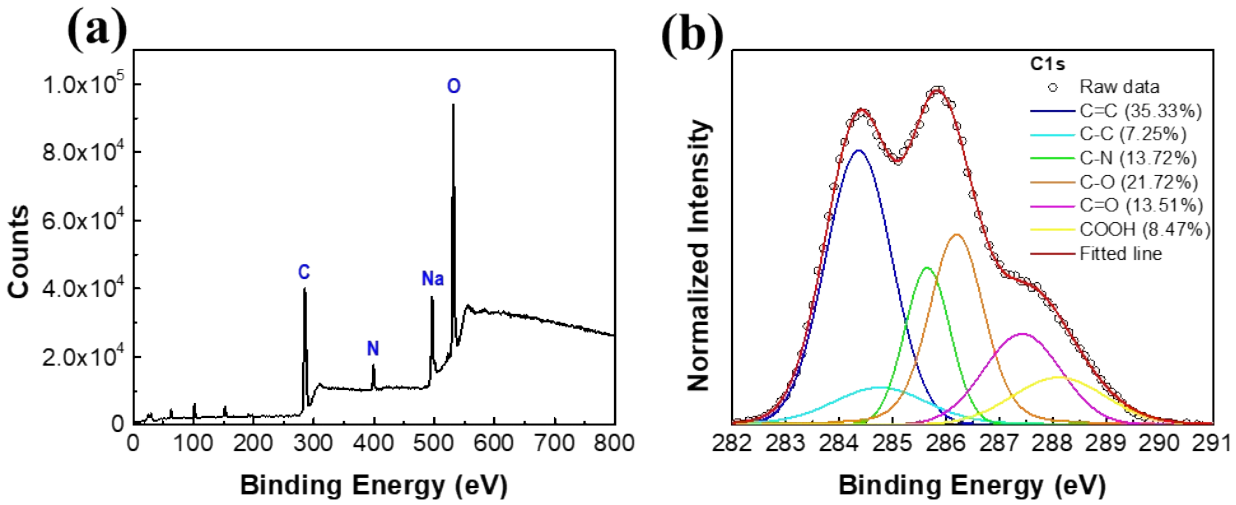

Figure S2. XPS (a) full and (b) narrow scans of NGQDs.

Figure S2a shows the full-scan XPS spectrum, where the C 1s, N 1s and O 1s peaks are located at 284.0, 398.1 and 531.1 eV, respectively. The observed sodium peak is due to the salts produced during the neutralization with NaOH in the purification process. In addition, high-resolution XPS (HRXPS) measurements were also conducted to study the bonding configurations in the NGQDs. From **Figure S2b**, it can be seen that the C 1s peak can be divided into six different peaks after deconvolution, comprising of C=C (284.4 eV), C-C (284.8 eV), C-N (285.6) eV), C-O (286.2 eV), C=N (287.4 eV) and COOH (288.1 eV).[5]

S4. Detection at LoD level

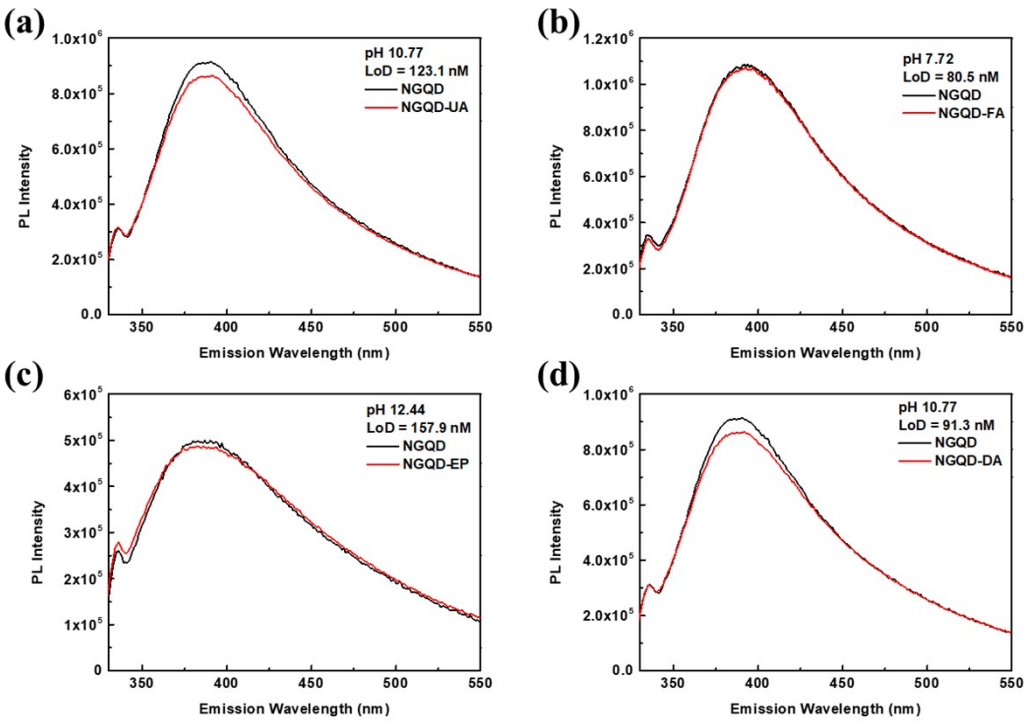

Figure S3. PL spectra of NGQDs with the presence of (a) 123.1 nm UA at pH 10.77 (b) 90.5 nm FA at pH 7.72 (c) 157.9 nm EP at pH 12.44 and (d) 91.3 nm DA at pH 10.77.

The estimated LoDs for those four biomarkers are within the detection range in human-related diseases, suggesting that the synthesized NGQDs have the potential for real-time monitoring of those biomarkers in human fluid. On the other hand, the addition of EP to the NGQD solution also produces a new PL peak at 545 nm (**Figure 5e**) referring to the emission of oxidized EP under alkaline conditions, [6] which is also beneficial for the qualitative detection purpose of EP.

S5. Comparison of the synthesized NGQDs with other literatures

Table S1. Comparison of UA, FA, EP and DA detections based on the synthesized NGQDs with different fluorescent materials.

Materials	Biomol.	Linear Range (µM)	R^2	LoD (nM)	Ref.
NGQDs	UA	0.8 – 50 50 – 100	0.997 0.998	97.7	This work
	FA	0.8 – 100	0.998	80.5	
	EP	0.6 – 50 50 – 100	0.995 0.997	56.4	
	DA	0.8 – 100	0.999	91.3	
CdZnTeS QDs	UA	100 – 900	0.997	20300	[7]
CdS QDs	UA	125 – 1000	0.992	125	[8]
ZnO QDs	UA	1000 – 10000	0.996	22900	[9]
S, N- CQDs	UA	0.05 – 1.5	0.999	17	[10]
CQDs	FA	1.14 – 47.57	0.99	380	[11]
CdTe/ZnS QDs	FA	0.1 – 50	0.975	200	[12]
MoS_2 QDs	FA	0.1 – 125	–	100	[13]
CdTeS QDs	FA	5 – 80	0.992	300	[14]
MQDs	EP	0.2 – 10 10 – 40	0.998 0.996	50	[15]
GQDs	EP	1 – 200	0.998	500	[16]
QDs@MIP	EP	0.08 - 20	0.992	12	[17]
S, N-CQDs	DA	0 - 50	0.991	82	[18]
NB-CQDs	DA	0.1 - 70	0.996	11	[19]
SiQDs	DA	0.83 – 83.33	> 0.99	320	[20]
N-CQDs	DA	0.25 - 30	0.996	97.2	[21]

S6. Interference studies

Table S2. Detection of UA, FA, DA, and EP in several different spiked samples.

Biomolecules	Specimen Concentration (μM)	Incubation time (min)	Goal Analysis	Measured concentration (μM)	RSD (%)
Mixture A					
UA	6				
Homocysteine	6				
Glycine	6				
GSH	6	5	UA	5.87 ± 0.61	2.21
Cysteine	6				
Glucose	6				
ATP	6				
Mixture B					
FA	6				
Homocysteine	6				
Glycine	6				
GSH	6	5	FA	6.08 ± 0.12	1.32
Cysteine	6				
Glucose	6				
ATP	6				
Mixture C					
EP	6				
Homocysteine	6				
Glycine	6	10	EP	6.17 ± 0.18	2.70
GSH	6				
Cysteine	6				

Glucose	6				
ATP	6				
Mixture D					
DA	6				
Homocysteine	6				
Glycine	6				
GSH	6	10	DA	5.99 ± 0.25	0.17
Cysteine	6				
Glucose	6				
ATP	6				
Mixture E					
UA	15				
FA	6				
EP	6				
DA	6				
Homocysteine	6				
Glycine	6	5	UA	14.83 ± 0.35	1.15
GSH	6				
Cysteine	6				
Glucose	6				
ATP	6				
Mixture F					
UA	15				
FA	2				
EP	2	5	FA	14.75 ± 0.30	1.69
DA	2				

Homocysteine	6				
Glycine	6				
GSH	6				
Cysteine	6				
Glucose	6				
ATP	6				
Mixture G					
FA	15				
UA	6				
EP	6				
DA	6				
Homocysteine	6	5	FA	15.28 ± 0.12	1.83
Glycine	6				
GSH	6				
Cysteine	6				
Glucose	6				
ATP	6				
Mixture H					
EP	15				
UA	6				
FA	6				
DA	6				
Homocysteine	6	10	EP	15.06 ± 0.13	0.40
Glycine	6				
GSH	6				
Cysteine	6				
Glucose	6				

ATP	6				
Mixture I					
DA	15	10	DA	15.39 ± 0.14	2.5
UA	6				
FA	6				
EP	6				
Homocysteine	6				
Glycine	6				
GSH	6				
Cysteine	6				
Glucose	6				
ATP	6				
Mixture J					
DA	15	10	DA	15.13 ± 0.16	0.86
UA	2				
FA	2				
EP	2				
Homocysteine	6				
Glycine	6				
GSH	6				
Cysteine	6				
Glucose	6				
ATP	6				

The concentrations of these interferences were set to 6 μM, respectively. For more complex measurements, different concentrations of UA, FA, EP and DA were further added to some of the mixtures. Mixtures A, E and F were used primarily to simulate the detection of UA; mixtures B and G were used to simulate the detection of FA; mixtures C and H were used for the detection of EP. Measurements were performed according to the optimal conditions for each biomarker, UA was pH 10.77, incubated for 5 minutes; FA was pH 7.72, incubated for 5 minutes; EP was pH 12.44, incubated for 10 minutes; DA was pH 10.77, incubated for 10 minutes.

In the actual detection process, biomarkers may exist in different concentrations, so we mixed the four biomarkers with the interfering substances at different concentrations to closely simulate the actual condition. Generally, UA exists in human urine, FA exists in human blood, and EP and DA exist in the central nervous and brain systems, thus we opted to increase the concentration of the targeted biomarkers. Measurements of mixtures E, G, H, and I have very low relative standard deviation (RSD) within 4%, indicating accurate measurement of targeted biomarkers. In addition, since the pH values for the measurements of UA and DA are the same, mixtures J and F were re-planned. As shown by the results, UA and DA can be distinguished by the difference in incubation time.

S7. Selective detection protocol

First, the PL measurements need to be performed above pH 10, where the presence of EP can be easily observed by the occurrence of a new peak at 545 nm. When no new emission wavelength is observed at 545 nm but there is still PL quenching of NGQDs, it can be concluded that the sample does not contain any EP, and the PL quenching can be caused due to the presence of UA or DA. To differentiate DA and UA, detection in different pH values are conducted. For DA, the pH value needs to be at 10.77 to give a significant quenching effect, there is almost no change at other pH values. Contrarily, UA can still give a quenching effect at other pH values although it is not as significant as at pH 10.77. Different incubation time strategy can also assist the differentiation of UA and DA. PL sensing in an alkaline environment (pH > 10) helps to discriminate the presence of EP, while in a neutral environment it can discriminate the presence of FA. Therefore, by following this protocol, rapid qualitative detection of UA, FA, EP and DA can be achieved simultaneously.

S8. Stability testing of NGQDs under different pH conditions

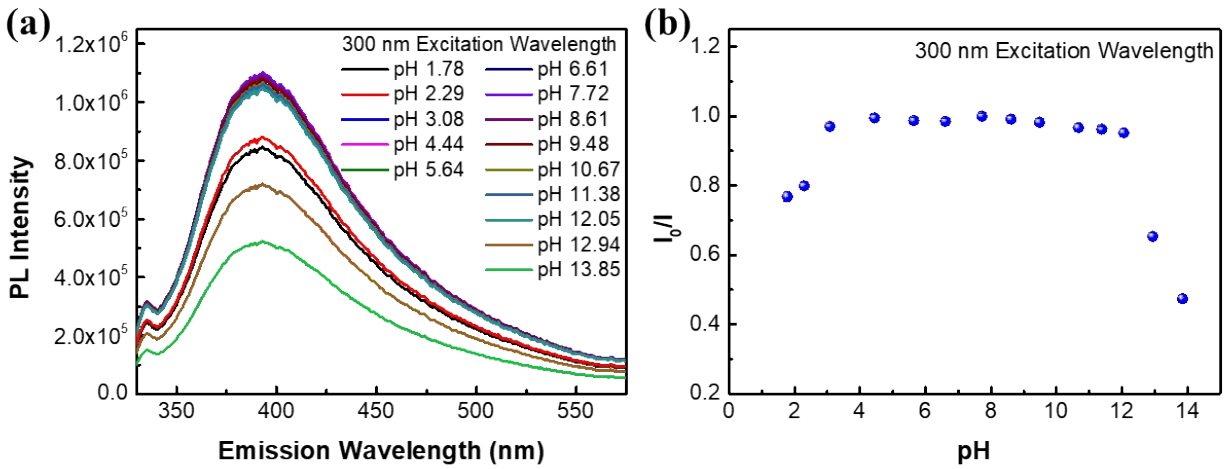

Figure S4. pH detection using NGQDs. (a) PL spectra of NGQDs solutions with different pH values under 300 nm excitation. (b) Plot of the pH values versus PL intensity ratio of I/I_0 of NGQDs in different pH values under 300 nm excitation.

The I_0 and I represent the PL intensities of NGQDs under 300 nm excitation at pH 7.72 (0.1 M PBS solutions) and at different pH values, respectively. Thus, when the I_0/I equals to ~1.0, it can be concluded that the PL intensity remains stable across different pH values. Based on the result, the emission intensity of NGQDs remained stable from pH 3.18 to 11.38, indicating that the synthesized NGQDs are relatively stable and have a great potential as biosensors.

S9. Sensing mechanisms

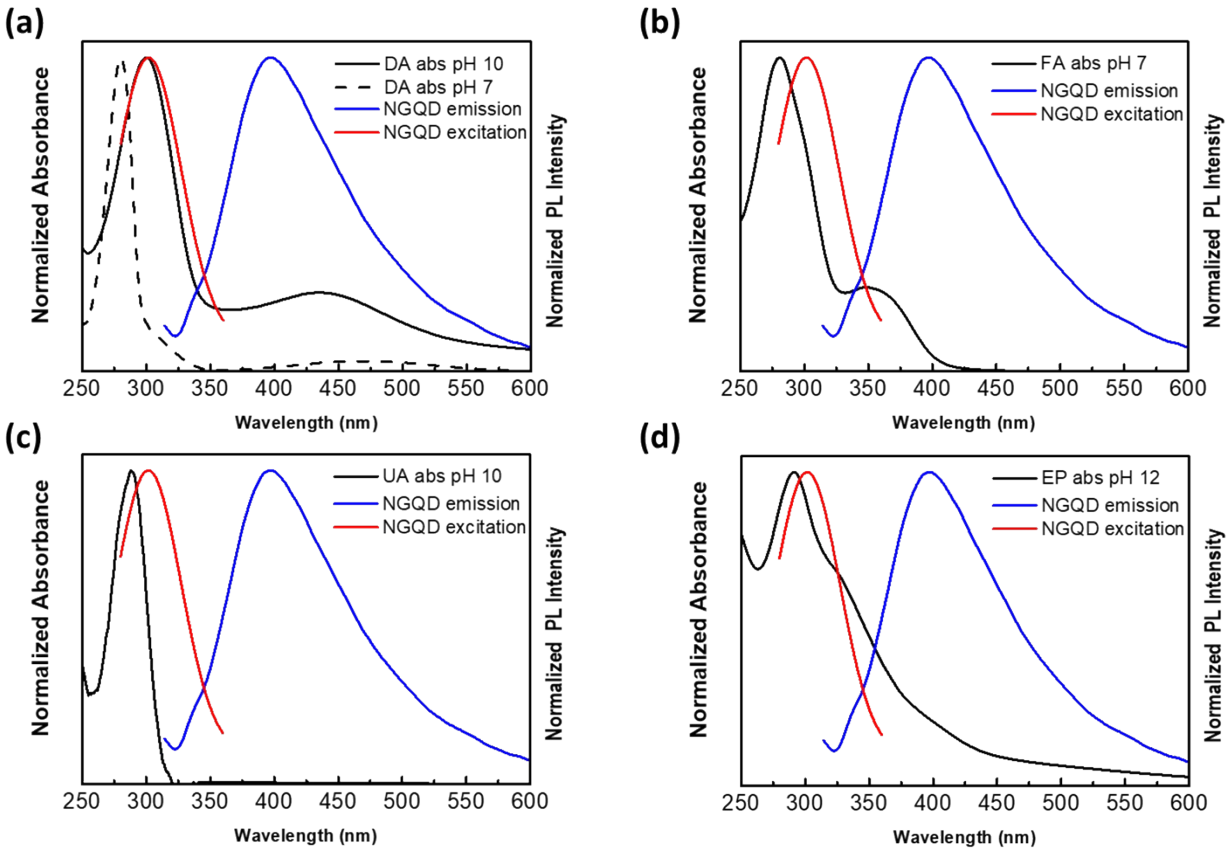

Figure S5. PL excitation and emission spectra of NGQDs as well as absorption spectra of (a) DA at pH 10 (solid line) and 7 (dash line), (b) FA at pH 7, (c) UA at pH 10, and (d) EP at pH 12.

References

[1] A. Zając, J. Hanuza, M. Wandas, L. Dymińska, Determination of N-acetylation degree in chitosan using Raman spectroscopy, Spectrochimica Acta Part A: Molecular and Biomolecular Spectroscopy, 134(2015) 114-20.

[2] S.H. Jin, D.H. Kim, G.H. Jun, S.H. Hong, S. Jeon, Tuning the photoluminescence of graphene quantum dots through the charge transfer effect of functional groups, ACS nano, 7(2013) 1239-45.

[3] X. Ye, Y. Xiang, Q. Wang, Z. Li, Z. Liu, A Red Emissive Two-Photon Fluorescence Probe Based on Carbon Dots for Intracellular pH Detection, Small, 15(2019) 1901673.

[4] X. Wen, L. Shi, G. Wen, Y. Li, C. Dong, J. Yang, et al., Green and facile synthesis of nitrogen-doped carbon nanodots for multicolor cellular imaging and Co2+ sensing in living cells, Sensors and Actuators B: Chemical, 235(2016) 179-87.

[5] D. Kurniawan, W.-H. Chiang, Microplasma-enabled colloidal nitrogen-doped graphene quantum dots for broad-range fluorescent pH sensors, Carbon, 167(2020) 675-84.

[6] Y. Wang, M. Yang, Y. Ren, J. Fan, Cu-Mn codoped ZnS quantum dots-based ratiometric fluorescent sensor for folic acid, Analytica chimica acta, 1040(2018) 136-42.

[7] F. Lu, Y. Yang, Y. Liu, F. Wang, X. Ji, Z. He, Point-of-care testing (POCT) of patients with a high concentration of uric acid by using alginate hydrogel microspheres embedded with CdZnTeS QDs and urate oxidase (Alg@ QDs-UOx MSs), Analyst, 146(2021) 949-55.

[8] N.E. Azmi, N.I. Ramli, J. Abdullah, M.A.A. Hamid, H. Sidek, S. Abd Rahman, et al., A simple and sensitive fluorescence based biosensor for the determination of uric acid using H2O2-sensitive quantum dots/dual enzymes, Biosensors and Bioelectronics, 67(2015) 129-33.

[9] M. Ali, I. Shah, S.W. Kim, M. Sajid, J.H. Lim, K.H. Choi, Quantitative detection of uric acid through ZnO quantum dots based highly sensitive electrochemical biosensor, Sensors and Actuators A: Physical, 283(2018) 282-90.

[10] T. Hallaj, M. Amjadi, F. Mirbirang, S, N-doped carbon quantum dots enhanced Luminol-Mn(IV) chemiluminescence reaction for detection of uric acid in biological fluids, Microchemical Journal, 156(2020) 104841.

[11] W. Zhang, B. Wu, Z. Li, Y. Wang, J. Zhou, Y. Li, Carbon quantum dots as fluorescence sensors for label-free detection of folic acid in biological samples, Spectrochimica Acta Part A: Molecular and Biomolecular Spectroscopy, 229(2020) 117931.

[12] S.K. Vaishanav, J. Korram, R. Nagwanshi, I. Karbhal, L. Dewangan, K.K. Ghosh, et al., Interaction of Folic Acid with Mn2+ Doped CdTe/ZnS Quantum Dots: In Situ Detection of Folic Acid, Journal of fluorescence, 31(2021) 951-60.

[13] Y. Peng, W. Dong, L. Wan, X. Quan, Determination of folic acid via its quenching effect on the fluorescence of MoS2 quantum dots, Microchimica Acta, 186(2019) 1-8.

[14] M. Yang, C. Wang, Y. Yan, E. Liu, X. Hu, H. Hao, et al., Visual detection of folic acid based on silica coated CdTeS quantum dots in serum samples, Materials Research Bulletin, 144(2021) 111509.

[15] F. Zhang, M. Wang, D. Zeng, H. Zhang, Y. Li, X. Su, A molybdenum disulfide quantum dots-based ratiometric fluorescence strategy for sensitive detection of epinephrine and ascorbic acid, Analytica Chimica Acta, 1089(2019) 123-30.
[16] M. Wang, Y. Li, L. Wang, X. Su, A label-free fluorescence nanosensor for the determination of adrenaline based on graphene quantum dots, Analytical Methods, 9(2017) 4434-8.
[17] F. Wei, G. Xu, Y. Wu, X. Wang, J. Yang, L. Liu, et al., Molecularly imprinted polymers on dual-color quantum dots for simultaneous detection of norepinephrine and epinephrine, Sensors and Actuators B: Chemical, 229(2016) 38-46.
[18] C. Wang, H. Shi, M. Yang, Z. Yao, B. Zhang, E. Liu, et al., Biocompatible sulfur nitrogen co-doped carbon quantum dots for highly sensitive and selective detection of dopamine, Colloids and Surfaces B: Biointerfaces, 205(2021) 111874.
[19] Y. Liu, W. Li, P. Wu, C. Ma, X. Wu, M. Xu, et al., Hydrothermal synthesis of nitrogen and boron co-doped carbon quantum dots for application in acetone and dopamine sensors and multicolor cellular imaging, Sensors and Actuators B: Chemical, 281(2019) 34-43.
[20] G.-Y. Chang, D. Kurniawan, Y.-J. Chang, W.-H. Chiang, Microplasma-Enabled Surfaced-Functionalized Silicon Quantum Dots for Label-Free Detection of Dopamine, ACS Omega, 7(2022) 223-9.
[21] C. Wang, H. Shi, M. Yang, Y. Yan, E. Liu, Z. Ji, et al., A novel nitrogen-doped carbon quantum dots as effective fluorescent probes for detecting dopamine, Journal of Photochemistry and Photobiology A: Chemistry, 391(2020) 112374.